Bound-waves due to sea and swell trigger the generation of freak-waves

David Andrade & Michael Stiassnie

Journal of Ocean Engineering and Marine Energy

ISSN 2198-6444

J. Ocean Eng. Mar. Energy
DOI 10.1007/s40722-020-00179-3

Springer

Your article is protected by copyright and all rights are held exclusively by Springer Nature Switzerland AG. This e-offprint is for personal use only and shall not be self-archived in electronic repositories. If you wish to self-archive your article, please use the accepted manuscript version for posting on your own website. You may further deposit the accepted manuscript version in any repository, provided it is only made publicly available 12 months after official publication or later and provided acknowledgement is given to the original source of publication and a link is inserted to the published article on Springer's website. The link must be accompanied by the following text: "The final publication is available at link.springer.com".

Author's personal copy

Journal of Ocean Engineering and Marine Energy
https://doi.org/10.1007/s40722-020-00179-3

RESEARCH ARTICLE

Bound-waves due to sea and swell trigger the generation of freak-waves

David Andrade[1] · Michael Stiassnie[1]

Received: 4 August 2020 / Accepted: 5 October 2020
© Springer Nature Switzerland AG 2020

Abstract
Averaged bound-waves, arising from the interaction of a stormy-sea with a marginal swell, are used as an initial inhomogeneous disturbance which, as a result of an instability inherent in narrow homogeneous JONSWAP spectra, is amplified exponentially. This drives the system away from the equilibrium. Finally, by looking into the statistics of the underlying sea state we find that, throughout the non linear long time evolution, there is an increase in the probability of freak wave occurrence.

Keywords Freak-waves · C.S.Y. equation · Inhomogeneous random waves · Bound-waves

1 Introduction

In this article, we propose a mechanism for the generation of freak waves in a sea state consisting of a local wind sea and a swell.

This mechanism is probabilistic in nature, i.e. it does not show how a freak wave would emerge out of a single realization of the surface elevation in combination with swell. Rather, it shows that throughout the non linear, long time evolution of the sea state, treated as a Gaussian process, the probability of extreme waves is increased considerably.

Dealing with non-linear random inhomogeneous waves is the crux of the matter.

In the context of deep water waves, there are currently two equations at hand. We have the Alber equation, see Alber (1978), and the equation derived by Crawford, Saffman and Yuen, see Crawford et al. (1980), that we call the C.S.Y. equation. The main difference is that Alber's equation is a narrow banded model whereas the C.S.Y. is not. Actually, Alber's equation can be derived directly from the C.S.Y. equation, see Crawford et al. (1980).

We choose the C.S.Y. equation as the model for non linear evolution of random inhomogeneous waves.

✉ David Andrade
deandradep@gmail.com

Michael Stiassnie
miky@technion.ac.il

[1] Department of Civil and Environmental Engineering, Technion, Haifa, Israel

There are two steps needed for the mechanism to generate freak waves. First, one must find the instability generator of the underlying wave spectrum. This means considering a special inhomogeneous perturbation of a homogeneous spectrum, defined in terms of a wave number and some frequencies. Whenever any of such frequencies have a non-zero imaginary part, the wave vector of the disturbance destabilizes the spectrum. The set of all such unstable wave vectors act as the instability generator of the spectrum.

Here is where the swell enters the picture. It turns out that, by taking two-wave vector correlations, between the bound-waves (arising from the sea and the swell) and the free waves of the sea, one obtains a similar type of inhomogeneous perturbation required as a generator of instability. The wave vector of the disturbance is the wave vector of the swell.

In case of a destabilizing swell, the next step is to compute the non linear, long time evolution of the spectrum. This is achieved by using a discretized version of the C.S.Y. equation as was done in Andrade and Stiassnie (2020). We look at the evolution of the wave spectrum, as it reveals energy exchange among the waves, and the variance of the free surface elevation, which shows how the average wave energy spreads across the space-time domain. Then following Regev et al. (2008), we use the time evolution of the variance to find increases in the probability of freak-wave occurrence.

It should be noted that it is already an established fact that it is likely to encounter freak-waves during the evolution of inhomogeneous wave fields. See Regev et al. (2008) or Ribal et al. (2013), for results obtained from Alber's equation. See

Published online: 23 October 2020

Author's personal copy

Stuhlmeier and Stiassnie (2019) and Andrade and Stiassnie (2020) for results based on the C.S.Y. equation.

Despite this, the main point of the current paper is to show one physical mechanism capable of triggering the increase in the freak-wave probability, thus the generation of freak-waves, namely the bound-waves arising from the interaction between the local sea and a swell.

The idea of using bound-waves as an inhomogeneous disturbance of a homogeneous spectrum was originally investigated in Regev et al. (2008). They used Alber's equation to establish their results. One of the novelties of this paper is that it uses the more general, broad-banded C.S.Y. equation.

2 Deterministic model: the Zakharov equation

In this article, we consider the non-linear, long time evolution of deep-water waves governed by the Zakharov equation:

$$\frac{\partial}{\partial t}B_0 = -i\iiint T_{0,1,2,3}\, B_1^* B_2 B_3\, \delta_{0,1}^{2,3}\, e^{i\,\Delta_{0,1}^{2,3} t}\, d\mathbf{k}_{1,2,3}. \quad (1)$$

Here subscripts denote a wave vector, so $B_0 = B(\mathbf{k}_0)$, etc. The kernel $T_{0,1,2,3}$ can be found in Krasitskii (1994) and Mei et al. (2018). The asterisk * denotes complex conjugation and unless explicitly stated the integration limits are from $-\infty$ to ∞. We use the deep water dispersion relation $\omega_0 = \sqrt{gk_0}$, where g is the gravity acceleration and $k_0 = \|\mathbf{k}_0\|$.

In this context, one calls the complex-valued function B the free-wave amplitude spectrum. $|B|^2$ is the wave action (energy/frequency) spectrum.

The Zakharov equation governs the energy exchange among the wave components due to resonant and quasi-resonant four-wave interactions. This is incorporated in the Dirac delta function $\delta_{0,1}^{2,3} = \delta(\mathbf{k}_0 + \mathbf{k}_1 - \mathbf{k}_2 - \mathbf{k}_3)$, together with the frequency detuning $\Delta_{0,1}^{2,3} = \omega_0 + \omega_1 - \omega_2 - \omega_3$, which marks the departure from exact resonance.

The free-wave spectrum B is the leading order approximation of the more general amplitude spectrum b. Actually, throughout the derivation of the Zakharov equation one uses the following expansion of the amplitude spectrum into free-waves and bound-waves

$$b(\mathbf{k}, t) = \left[B(\mathbf{k}, t) + B'(\mathbf{k}, t) + \cdots\right] e^{-i\omega t}. \quad (2)$$

Let ε be a typical steepness of the wave field. Then the free-waves $B = \mathcal{O}(\varepsilon)$ and the bound-waves $B' = \mathcal{O}(\varepsilon^2)$. The full expansion of the amplitude spectrum b also includes higher order bound-waves such as $B'' = \mathcal{O}(\varepsilon^3)$, see Mei et al. (2018). In this article, we only consider the leading bound-wave spectrum B'.

It turns out that the bound-waves are determined by the free waves. Specifically, one has the following equation for B' in terms of B:

$$\begin{aligned} B_0' = &-\iint \frac{V_{0,1,2}^{(1)}}{\omega_0 - \omega_1 - \omega_2}\, B_1 B_2\, e^{i(\omega_0-\omega_1-\omega_2)t}\, \delta_{0-1-2}\, d\mathbf{k}_{1,2} \\ &-\iint \frac{V_{0,1,2}^{(2)}}{\omega_0 + \omega_1 - \omega_2}\, B_1^* B_2\, e^{i(\omega_0+\omega_1-\omega_2)t}\, \delta_{0+1-2}\, d\mathbf{k}_{1,2} \\ &-\iint \frac{V_{0,1,2}^{(3)}}{\omega_0 + \omega_1 + \omega_2}\, B_1^* B_2^*\, e^{i(\omega_0+\omega_1+\omega_2)t}\, \delta_{0+1+2}\, d\mathbf{k}_{1,2}. \end{aligned} \quad (3)$$

All the kernels can be found in Mei et al. (2018).

Note that the Zakharov equation is a deterministic model; predictions can only be made provided that one is given some initial conditions. In some applications obtaining exact initial conditions is not feasible, as it would require exact knowledge of the ocean surface elevation, and its speed, at a specific instant. Therefore in order to make predictions out of Zakharov's equation we turn to its leading order stochastic counterpart, the C.S.Y. equation.

3 Stochastic model: the C.S.Y. equation

Randomness is introduced into the system by letting the free-wave amplitude spectrum to be a mean zero Gaussian stochastic process. We use $\langle\cdot\rangle$ to denote an ensemble average.

We shall be primarily concerned with the determination of the second order moments of the process, which are the values of the two-wave-vector spectral correlation function[1]

$$R_{ij}(t) = \langle B(\mathbf{k}_i, t) B^*(\mathbf{k}_j, t)\rangle. \quad (4)$$

Directly from Zakharov equation and under the assumption of strict Gaussianity, Crawford, Saffman and Yuen derived, the following equation for R, known as the C.S.Y. equation, see Crawford et al. (1980).

$$\begin{aligned} \frac{\partial}{\partial t}R_{ij} = &-2i\iiint T_{i,m,n,p}\delta_{i,m}^{n,p} e^{i\,\Delta_{i,m}^{n,p} t} R_{nj} R_{pm}\, d\mathbf{k}_{m,n,p} \\ &+ 2i\iiint T_{j,m,n,p}\delta_{j,m}^{n,p} e^{-i\,\Delta_{j,m}^{n,p} t} R_{in} R_{mp}\, d\mathbf{k}_{m,n,p}. \end{aligned} \quad (5)$$

It is convenient to define

$$r_{ij} = \mathrm{e}^{-i(\omega_i-\omega_j)t} R_{ij}, \quad (6)$$

[1] All correlations of the form $\langle B(\mathbf{k}_i) B(\mathbf{k}_j)\rangle$ are assumed to be zero.

Author's personal copy

and rewrite equation (5) as

$$\begin{aligned}\frac{\partial}{\partial t}r_{ij} &= -i\left(\omega_i-\omega_j\right)r_{ij}\\ &\quad -2i\iint T_{i,m,n,p}\delta^{n,p}_{i,m}r_{nj}r_{pm}\,d\mathbf{k}_{m,n,p}\\ &\quad +2i\iint T_{j,m,n,p}\delta^{n,p}_{j,m}r_{in}r_{mp}\,d\mathbf{k}_{m,n,p}.\end{aligned}\tag{7}$$

3.1 Homogeneous solutions

There is an important class of solutions of the C.S.Y. equation which are called homogeneous solutions. Such solutions have a correlation function of the form

$$R_{ij}=C_i\delta(\mathbf{k}_i-\mathbf{k}_j).\tag{8}$$

By substituting (8) into Eq. (5) it can be shown that any homogeneous solution is stationary. Note that in this case $R_{jj}=r_{jj}$.

Given a wave $\mathbf{k}_j$, the value $C_j=\langle|B_j|^2\rangle$ is the average wave action of the wave $\mathbf{k}_j$. Thus one refers to C_j as the wave action spectrum.

The fact that homogeneous solutions are stationary implies that a non-trivial time evolution of a given (homogeneous) wave action spectrum is only possible when there are inhomogeneous perturbations in the initial conditions. Hence, one asks how unstable is a homogeneous spectrum to inhomogeneous disturbances? We turn to this matter next.

3.2 Linearized C.S.Y. equation

Given a homogeneous wave action spectrum C_j one is interested in studying its instability to initial inhomogeneous disturbances. To this end, one looks for short-time solutions of the form

$$r_{ij}(t)=C_i\delta(\mathbf{k}_i-\mathbf{k}_j)+r^{(1)}_{ij}(t)+\cdots.\tag{9}$$

Upon substituting this expression into (7) and collecting the linear terms in $r^{(1)}_{ij}$, one gets the following linear equation for $r^{(1)}_{ij}$:

$$\begin{aligned}\frac{\partial}{\partial t}r^{(1)}_{ij} &= -i\left(\Omega_i-\Omega_j\right)r^{(1)}_{ij}\\ &\quad +2i(C_i-C_j)\iint T_{i,m,j,n}\,\delta^{j,n}_{i,m}\,r^{(1)}_{nm}\,d\mathbf{k}_{n,m},\end{aligned}\tag{10}$$

where the function Ω is

$$\Omega_0=\omega_0+2\int T_{0,m,0,m}C_m\,d\mathbf{k}_m.\tag{11}$$

Note that Eq. (10) is valid for every $\mathbf{k}_i$ and $\mathbf{k}_j$. It is linear since the values of the wave action spectrum C_j are given. When $\mathbf{k}_i=\mathbf{k}_j$, $\partial r^{(1)}_{jj}/\partial t=0$. We take $r^{(1)}_{jj}=0$ without any loss of generality.

Equation (10) is the continuous version of equation (19) studied in Andrade and Stiassnie (2020) in the discrete case.

Next, one introduces new variables by letting

$$\mathbf{m}=\left(\mathbf{k}_i+\mathbf{k}_j\right)/2.\tag{12}$$

$$\mathbf{n}=\mathbf{k}_i-\mathbf{k}_j.\tag{13}$$

$$F(\mathbf{m},\mathbf{n},t)=r(\mathbf{m}+\mathbf{n}/2,\mathbf{m}-\mathbf{n}/2,t).\tag{14}$$

In terms of F, Eq. (10) becomes

$$\begin{aligned}\frac{d}{dt}F &= -i\left(\Omega(\mathbf{m}+\mathbf{n}/2)-\Omega(\mathbf{m}-\mathbf{n}/2)\right)F\\ &\quad +2i(C(\mathbf{m}+\mathbf{n}/2)-C(\mathbf{m}-\mathbf{n}/2))\\ &\quad \times\iint T(\mathbf{m}+\mathbf{n}/2,\mathbf{u}-\mathbf{v}/2,\mathbf{m}-\mathbf{n}/2,\mathbf{u}+\mathbf{v}/2)\\ &\quad \times\delta^{\mathbf{v}}_{\mathbf{n}}F(\mathbf{u},\mathbf{v})\,d\mathbf{u}d\mathbf{v}.\end{aligned}\tag{15}$$

Here, in the integral on the right-hand side of (10), we substituted the dummy variables of integration $\mathbf{k}_m$ and $\mathbf{k}_n$ by new variables $\mathbf{u}=(\mathbf{k}_m+\mathbf{k}_n)/2$ and $\mathbf{v}=\mathbf{k}_n-\mathbf{k}_m$.

Next one integrates the delta function on the right-hand side of equation (15) obtaining

$$\begin{aligned}\frac{d}{dt}F &= -i\left(\Omega(\mathbf{m}+\mathbf{n}/2)-\Omega(\mathbf{m}-\mathbf{n}/2)\right)F\\ &\quad +2i(C(\mathbf{m}+\mathbf{n}/2)-C(\mathbf{m}-\mathbf{n}/2))\\ &\quad \times\int T(\mathbf{m}+\mathbf{n}/2,\mathbf{u}-\mathbf{n}/2,\mathbf{m}-\mathbf{n}/2,\mathbf{u}+\mathbf{n}/2)\\ &\quad \times F(\mathbf{u},\mathbf{n})\,d\mathbf{u}.\end{aligned}\tag{16}$$

Note that Eq. (16) is equivalent to equation (10), since we just changed variables.

The next step is to look for inhomogeneous solutions of the form:

$$\begin{aligned}F(\mathbf{m},\mathbf{n},t) = {}& e^{i\lambda t}M(\mathbf{m})\delta(\mathbf{n}-\mathbf{k}_L)\\ &+e^{-i\lambda t}M^*(\mathbf{m})\delta(\mathbf{n}+\mathbf{k}_L),\end{aligned}\tag{17}$$

where $M(\mathbf{m})$ is an arbitrary function, $\mathbf{k}_L$ is an arbitrary wave vector[2] and λ is a constant.

This ansatz is based on a previous experience with the discretized C.S.Y. equation. Note that, by reverting back

[2] Later on when working with JONSWAP spectrum the wave vector $\mathbf{k}_L$ will be the wave vector of a "long" wave, i.e., a swell; hence, the subscript.

Author's personal copy

to the wave vectors $\mathbf{k}_i$ and $\mathbf{k}_j$, one can see that the support of F consists of wave vectors of the form $\mathbf{k}_i - \mathbf{k}_j = \pm\mathbf{k}_L$, or in the new variables, $\mathbf{n} = \pm\mathbf{k}_L$. This property is shared with the eigenvalues of the linear discretized C.S.Y. equation studied in Andrade and Stiassnie (2020).

Substituting (17) into (16) and collecting the terms that have $\delta(\mathbf{n} - \mathbf{k}_L)$ as a common factor yields

$$\begin{aligned}(\lambda + \Omega(\mathbf{m} + \mathbf{k}_L/2) - \Omega(\mathbf{m} - \mathbf{k}_L/2))\, M(\mathbf{m}) \\ = 2(C(\mathbf{m} + \mathbf{k}_L/2) - C(\mathbf{m} - \mathbf{k}_L/2)) \\ \times \int T(\mathbf{m} + \mathbf{k}_L/2, \mathbf{u} - \mathbf{k}_L/2, \mathbf{m} \\ - \mathbf{k}_L/2, \mathbf{u} + \mathbf{k}_L/2) M(\mathbf{u})\, d\mathbf{u}.\end{aligned} \tag{18}$$

Equation (18) is a linear integral equation for M with λ appearing as an unknown parameter. It admits non trivial solutions ($M \neq 0$) depending on λ, which plays the role of an eigenvalue of the system.

Moreover, the behavior of the linear solution (17) is also determined by λ. It grows exponentially whenever $\mathrm{Im}[\lambda] \neq 0$. Otherwise, it oscillates in time.

Note that there is no need to consider the terms with $\delta(\mathbf{n} + \mathbf{k}_L)$, as they yield the same Eq. (18).

Equation (18) is remarkably similar to the one obtained in Badulin et al. (1995) for the instability problem of deterministic short-crested water waves to higher order harmonics.

One final remark concerning Eq. (18) is that, by taking its narrow-band approximation, as done in Crawford et al. (1980), one obtains equation (4.10) in Alber (1978), or equation (53) in Crawford et al. (1980). In this limit Eq. (18) simplifies, it becomes an equation for λ independent of M. This has been used as the starting point in several investigations regarding the instability of a homogeneous spectrum, see Stiassnie et al. (2008) and Ribal et al. (2013). Recently, it was studied using of the Wigner transform and the non-linear Schrödinger equation, see Athanassoulis et al. (2017).

3.3 Solving equation (18)

Given a wave action spectrum C and a wave vector $\mathbf{k}_L$, our goal is to find solutions of Eq. (18). This involves two tasks. First, to determine all λ such that a non-zero solution exists; then find the solution $M(\mathbf{m})$. All of this will be accomplished in the special case of a discrete wave action spectrum.

The spectrum is discretized by fixing N wave vectors $\mathbf{k}_1, \ldots, \mathbf{k}_N$, and replacing the continuous spectrum by a sum of Dirac deltas:

$$C(\mathbf{k}) = \sum_{n=1}^{N} C_n \delta(\mathbf{k} - \mathbf{k}_n). \tag{19}$$

Likewise we use the following ansatz for M:

$$\begin{aligned}M(\mathbf{m}) = \sum_{j=1}^{N} M_j^m \delta(\mathbf{m} - (\mathbf{k}_j - \mathbf{k}_L/2)) \\ + \sum_{j=1}^{N} M_j^p \delta(\mathbf{m} - (\mathbf{k}_j + \mathbf{k}_L/2)).\end{aligned} \tag{20}$$

The discrete counterpart of the integral equation (18) is the following linear system of $2N$ equations for the $2N$ unknowns $M_1^m, \ldots, M_N^m$ and $M_1^p, \ldots, M_N^p$:

$$\begin{aligned}(\lambda + \Omega(\mathbf{k}_i) - \Omega(\mathbf{k}_i - \mathbf{k}_L))\, M_i^m \\ = 2C_i \sum_{j=1}^{N} M_j^m T_{i,j-k,i-k,j} + M_j^p T_{i,j,i-k,j+k}.\end{aligned} \tag{21}$$

$$\begin{aligned}(\lambda + \Omega(\mathbf{k}_i + \mathbf{k}_L) - \Omega(\mathbf{k}_i))\, M_i^p \\ = -2C_i \sum_{j=1}^{N} M_j^m T_{i+k,j-k,i,j} + M_j^p T_{i+k,j,i,j+k}.\end{aligned} \tag{22}$$

In these equations, the index i runs from $1, \ldots, N$ and the subscript k stands for the wave vector $\mathbf{k}_L$ thus, $T_{i,j-k,i-k,j} = T(\mathbf{k}_i, \mathbf{k}_j - \mathbf{k}_L, \mathbf{k}_i - \mathbf{k}_L, \mathbf{k}_j)$, etc.

All the technical details regarding the derivation of Eqs. (21) and (22) from Eq. (18) are given in Appendix A.

Equations (21) and (22) admit non-trivial solutions when λ is an eigenvalue of the system. There are at most $2N$ different and possibly complex eigenvalues.

Once an eigenvalue is chosen, one may solve (21) and (22) for M_i^p and M_i^m and recover the function $M(\mathbf{m})$ from Eq. (20). Ultimately, by means of Eq. (17), one gets a solution of the linear C.S.Y. equation.

Note that the behavior of the solution given by Eq. (17) is determined by λ; it grows exponentially when $\mathrm{Im}[\lambda] \neq 0$, otherwise it oscillates in time. Hence one defines a growth rate by

$$G = \mathrm{Im}[\lambda], \quad \text{for } \lambda \text{ an eigenvalue of (21) and (22).} \tag{23}$$

Given a spectrum C and a wave vector $\mathbf{k}_L$, we say that it is unstable provided that the system (21) and (22) has at least one growth rate.

In practice, it suffices to look for eigenvalues with positive imaginary part, since when λ is an eigenvalue, so is its complex conjugate λ^*.

Author's personal copy

4 Instability of JONSWAP spectrum

Now we apply the theoretical results obtained in the previous section and study the instabilities of a sea state given by a unidirectional JONSWAP spectrum.

The energy spectrum of the sea is given by

$$S(k) = \frac{\alpha}{2k^3} \exp\left[-\frac{5}{4}\left(\frac{k}{k_p}\right)^{-2}\right] \gamma^{\exp\left[-\left(\sqrt{\frac{k}{k_p}}-1\right)^2/2\sigma^2\right]}, \tag{24}$$

where $\mathbf{k} = (k, 0)$. Moreover, we set the following parameters: $k_p = 1$ and $\sigma = 0.08$.

A typical steepness of the wave field is

$$\varepsilon = k_p \sqrt{2 \int S(k)\, dk}. \tag{25}$$

The values of α, γ and ε used herein are given in Table 1. These correspond to cases a and b investigated in Andrade and Stiassnie (2020).

The energy spectrum is discretized as a sum of Dirac's delta functions:

$$S(\mathbf{k}) = \sum_{j=1}^{N} S_j\, \delta(\mathbf{k} - \mathbf{k}_j), \tag{26}$$

where the wave vectors $\mathbf{k}_j = (k_j, 0)$ are evenly spaced over the interval $[0, 4k_p]$. Let dk denote the spacing between consecutive wave numbers. In the following investigations we use a total of $N = 600$ wave numbers for the spectrum of the sea.

The initial wave action spectrum is

$$C_j = \frac{4g\pi^2 dk}{\omega_j} S_j, \tag{27}$$

as was used in Andrade and Stiassnie (2020).

In order to compute the growth rates we define a column vector $[M_1^m, \ldots, M_N^m, M_1^p, \ldots, M_N^p]^T$ and rewrite the system of Eqs. (21) and (22) in matrix form. Then we use MATLAB's eig routine to compute the eigenvalues of the system and the growth rates.

For every wave vector $\mathbf{k}_L$, there are at most 1200 different growth rates. However in order to test for the instability of the spectrum only one positive growth rate is needed. Thus from here on let G be the maximum growth rate. If $G > 0$ there is instability. Otherwise the spectrum is stable with respect to $\mathbf{k}_L$.

It is convenient to render all wave numbers and growth rates dimensionless by means of

$$\tilde{\mathbf{k}}_L = \frac{\mathbf{k}_L}{\varepsilon k_p}. \tag{28}$$

$$\tilde{G} = \frac{G}{\varepsilon^2 \omega_p}. \tag{29}$$

In Figs. 1 and 2, we plot the level lines $\tilde{G}$ as a function of the components of the dimensionless wave vector $\tilde{\mathbf{k}}_L = (\tilde{\mathbf{k}}_{L_x}, \tilde{\mathbf{k}}_{L_y})$. In both cases the instability region is bounded by a critical straight line that makes an angle of 25.64° with the x-axis for case A and 27.47° for case B. Also one can see that, the most unstable wave vector is along the x-axis.

Considering a wave vector with reflected components, i.e. $\mathbf{k}_L = (\mathbf{k}_{L_x}, -\mathbf{k}_{L_y})$, the corresponding instability region is flipped upside down; mirror reflection of Figs. 1 and 2. Moreover the system of Eqs. (21) and (22) is unchanged if one replaces $\mathbf{k}_L$ by $-\mathbf{k}_L$. This shows that the instability region for $-\mathbf{k}_L$ is also symmetrical with respect to the origin. These regions are remarkably similar to those regions of instability of a periodic wave train, in the deterministic case, shown in Yuen and Lake (1982).

Table 1 Parameters of the energy spectrum of the sea and of the swell used in the simulations

Cases	Sea				Swell		Growth rate
	α	γ	ε	H_s	a_L	k_L	$\tilde{G}$
Case A1	0.03	10	0.1787	0.5055 m	1 cm	0.0867 m^{-1}	0.1206
Case A2	0.03	10	0.1787	0.5055 m	1 cm	0.1733 m^{-1}	0.2231
Case A3	0.03	10	0.1787	0.5055 m	1 cm	0.34 m^{-1}	0.3204
Case A4	0.03	10	0.1787	0.5055 m	1 mm	0.34 m^{-1}	0.3204
Case A5	0.03	10	0.1787	0.5055 m	1 cm	0.5133 m^{-1}	0.1685
Case B1	0.015	20	0.1597	0.4518 m	1 cm	0.08 m^{-1}	0.1082
Case B2	0.015	20	0.1597	0.4518 m	1 cm	0.16 m^{-1}	0.3521
Case B3	0.015	20	0.1597	0.4518 m	1 cm	0.32 m^{-1}	0.3868
Case B4	0.015	20	0.1597	0.4518 m	1 mm	0.32 m^{-1}	0.3868
Case B5	0.015	20	0.1597	0.4518 m	1 cm	0.48 m^{-1}	0.1952

Author's personal copy

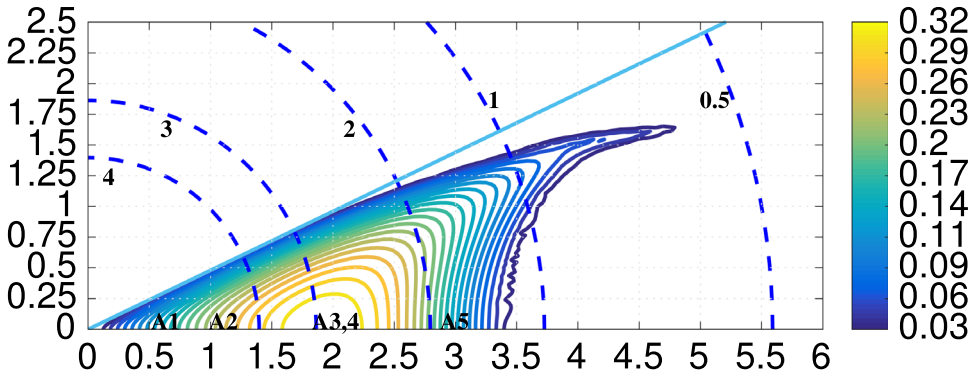

Fig. 1 Case A: instability region of the JONSWAP spectrum $\gamma = 10$ and $\alpha = 0.03$. The figure shows the level lines of $\tilde{G}$ as a function of the dimensionless wave vector $\tilde{\mathbf{k}}_L = (\tilde{\mathbf{k}}_{L_x}, \tilde{\mathbf{k}}_{L_y})$. The critical line is at an angle of 25.64°. The circular lines show the values of $\lambda_L/\lambda_p = 0.5, 1, 2, 3, 4$

The circular broken lines correspond to different values of

$$\frac{\lambda_L}{\lambda_p} = \varepsilon^{-1}\tilde{k}_L = c, \tag{30}$$

where λ_L and λ_p are the wavelengths of the long wave $\mathbf{k}_L$ and the peak wave $\mathbf{k}_p$, respectively. The values of the constant c are 0.5, 1, 2, 3 and 4.

As a consistency check, we compared our growth rates, obtained when $\mathbf{k}_L$ is on the grid points used to discretize the spectrum, against the values reported in Fig. 2b and Table 1 in Andrade and Stiassnie (2020). There was no noticeable difference between both computations.

5 Long time evolution

In this section we study the non-linear, long-time evolution of wave spectra. To this end, we compute numerical solutions of the C.S.Y. equation.

Note that, in order to start the evolution, some initial conditions are required, namely the initial wave action spectrum together with an inhomogeneous disturbance.

The mechanism to generate the disturbance is through the bound-waves between a local sea and a swell. We address this next.

5.1 Bound-wave correlation

Let us go back to the Zakharov equation. Recall that there is an amplitude spectrum $b(\mathbf{k})$ which decomposes into the free-wave spectrum $B(\mathbf{k})$ and (to leading order) a bound-wave spectrum $B'(\mathbf{k})$.

In order to model a local wind sea state and a swell, one decomposes the free wave spectrum as the sum of a sea state and a monochromatic swell:

$$B(\mathbf{k}, t) = B_L(t)\delta(\mathbf{k} - \mathbf{k}_L) + B_S(\mathbf{k}, t). \tag{31}$$

From now on $\mathbf{k}_L$ is the swell's wave vector. We use the subscript "L" for long and "S" for short.

Substituting (31) into (3), at $t = 0$, yields:

$$\begin{aligned}
B'(\mathbf{k}) = &-B_L \frac{V^{(1)}_{\mathbf{k},\mathbf{k}_L,\mathbf{k}-\mathbf{k}_L} + V^{(1)}_{\mathbf{k},\mathbf{k}-\mathbf{k}_L,\mathbf{k}_L}}{\omega(\mathbf{k}) - \omega(\mathbf{k}_L) - \omega(\mathbf{k}-\mathbf{k}_L)} B_S(\mathbf{k}-\mathbf{k}_L) \\
&- \int \frac{V^{(1)}_{\mathbf{k},\mathbf{k}_m,\mathbf{k}-\mathbf{k}_m}}{\omega(\mathbf{k}) - \omega(\mathbf{k}_m) - \omega(\mathbf{k}-\mathbf{k}_m)} B_S(\mathbf{k}_m) B_S(\mathbf{k}-\mathbf{k}_m)\, d\mathbf{k}_m \\
&- B^*_L \frac{V^{(2)}_{\mathbf{k},\mathbf{k}_L,\mathbf{k}+\mathbf{k}_L}}{\omega(\mathbf{k}) + \omega(\mathbf{k}_L) - \omega(\mathbf{k}+\mathbf{k}_L)} B_S(\mathbf{k}+\mathbf{k}_L) \\
&- B_L \frac{V^{(2)}_{\mathbf{k},\mathbf{k}_L-\mathbf{k},\mathbf{k}_L}}{\omega(\mathbf{k}) + \omega(\mathbf{k}_L-\mathbf{k}) - \omega(\mathbf{k}_L)} B^*_S(\mathbf{k}_L-\mathbf{k}) \\
&- \int \frac{V^{(2)}_{\mathbf{k},\mathbf{k}_m,\mathbf{k}+\mathbf{k}_m}}{\omega(\mathbf{k}) + \omega(\mathbf{k}_m) - \omega(\mathbf{k}+\mathbf{k}_m)} B^*_S(\mathbf{k}_m) B_S(\mathbf{k}+\mathbf{k}_m)\, d\mathbf{k}_m \\
&- B^*_L \frac{V^{(3)}_{\mathbf{k},\mathbf{k}_L,-(\mathbf{k}+\mathbf{k}_L)} + V^{(3)}_{\mathbf{k},-(\mathbf{k}+\mathbf{k}_L),\mathbf{k}_L}}{\omega(\mathbf{k}) + \omega(\mathbf{k}_L) + \omega(\mathbf{k}+\mathbf{k}_L)} B^*_S(-\mathbf{k}-\mathbf{k}_L) \\
&- \int \frac{V^{(3)}_{\mathbf{k},\mathbf{k}_m,-\mathbf{k}-\mathbf{k}_m}}{\omega(\mathbf{k}) + \omega(\mathbf{k}_m) + \omega(\mathbf{k}+\mathbf{k}_m)} B^*_S(\mathbf{k}_m) B^*_S(-\mathbf{k}-\mathbf{k}_m)\, d\mathbf{k}_m.
\end{aligned} \tag{32}$$

One introduces randomness in the system by letting the free-waves of the sea be a homogeneous Gaussian stochastic process with zero mean. Let $\langle\cdot\rangle$ be an ensemble average. Let us temporarily make the homogeneity assumption, so that:

$$\langle B_S(\mathbf{k}_i) B^*_S(\mathbf{k}_j)\rangle = C_j \delta(\mathbf{k}_i - \mathbf{k}_j). \tag{33}$$

The zero mean assumption implies that $\langle B_S(\mathbf{k}) B^*_L\rangle = 0$ for every $\mathbf{k}$, as B_L is a deterministic quantity.

In view of the expansion of the complex amplitude (2), it is readily seen that b itself is a stochastic process with mean $\langle b(\mathbf{k})\rangle = B_L\delta(\mathbf{k}-\mathbf{k}_L)$. Its two-wave-vector correlation function is:

$$\begin{aligned}
\langle b(\mathbf{k}_i) b^*(\mathbf{k}_j)\rangle = &\langle B(\mathbf{k}_i) B^*(\mathbf{k}_j)\rangle \\
&+ \langle B(\mathbf{k}_i)(B'(\mathbf{k}_j))^*\rangle \\
&+ \langle B'(\mathbf{k}_i) B^*(\mathbf{k}_j)\rangle) \\
&+ \langle B'(\mathbf{k}_i)(B'(\mathbf{k}_j))^*\rangle.
\end{aligned} \tag{34}$$

Author's personal copy

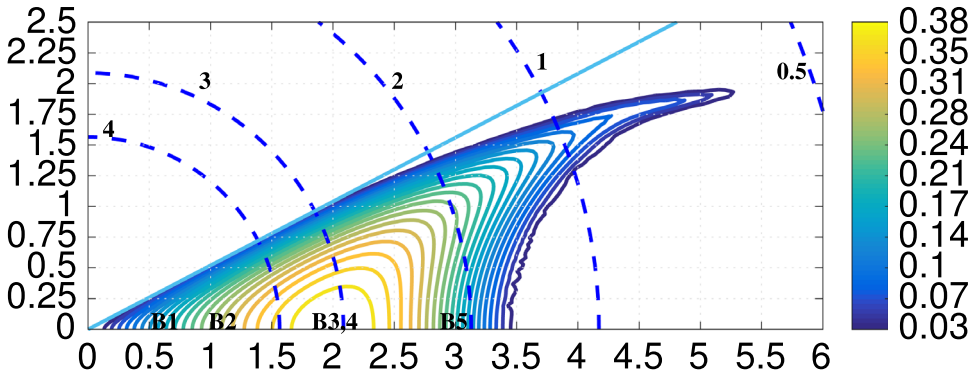

Fig. 2 Case B: instability region of the JONSWAP spectrum $\gamma = 20$ and $\alpha = 0.015$. The figure shows the level lines of $\tilde{G}$ as a function of the dimensionless wave vector $\tilde{\mathbf{k}}_L = (\tilde{\mathbf{k}}_{L_x}, \tilde{\mathbf{k}}_{L_y})$. The critical line is at an angle of 27.47°. The circular lines show the values of $\lambda_L/\lambda_p = 0.5, 1, 2, 3, 4$

Substituting (31) and (32) into (34) and keeping only leading order terms in B_L gives the following equation for the correlation function:

$$\begin{aligned}\langle b(\mathbf{k}_i)b^*(\mathbf{k}_j)\rangle &= |B_L|^2\delta(\mathbf{k}_i-\mathbf{k}_L)\delta(\mathbf{k}_j-\mathbf{k}_L)\\ &+ C(\mathbf{k}_i)\delta(\mathbf{k}_i-\mathbf{k}_j)\\ &- B_L\frac{V^{(1)}_{\mathbf{k}_i,\mathbf{k}_L,\mathbf{k}_j}+V^{(1)}_{\mathbf{k}_i,\mathbf{k}_j,\mathbf{k}_L}}{\omega(\mathbf{k}_i)-\omega(\mathbf{k}_L)-\omega(\mathbf{k}_j)}C(\mathbf{k}_j)\,\delta(\mathbf{k}_i-\mathbf{k}_j-\mathbf{k}_L)\\ &- B_L^*\frac{V^{(1)}_{\mathbf{k}_j,\mathbf{k}_L,\mathbf{k}_i}+V^{(1)}_{\mathbf{k}_j,\mathbf{k}_i,\mathbf{k}_L}}{\omega(\mathbf{k}_j)-\omega(\mathbf{k}_L)-\omega(\mathbf{k}_i)}C(\mathbf{k}_i)\,\delta(\mathbf{k}_j-\mathbf{k}_i-\mathbf{k}_L)\\ &- B_L^*\frac{V^{(2)}_{\mathbf{k}_i,\mathbf{k}_L,\mathbf{k}_j}}{\omega(\mathbf{k}_i)+\omega(\mathbf{k}_L)-\omega(\mathbf{k}_j)}C(\mathbf{k}_j)\,\delta(\mathbf{k}_i-\mathbf{k}_j+\mathbf{k}_L)\\ &- B_L\frac{V^{(2)}_{\mathbf{k}_j,\mathbf{k}_L,\mathbf{k}_i}}{\omega(\mathbf{k}_j)+\omega(\mathbf{k}_L)-\omega(\mathbf{k}_i)}C(\mathbf{k}_i)\,\delta(\mathbf{k}_j-\mathbf{k}_i+\mathbf{k}_L).\end{aligned} \tag{35}$$

In the inhomogeneous case, due to the decomposition (31), the two-wave-vector correlation function becomes:

$$\langle B_i B_j^*\rangle = |B_L|^2\delta(\mathbf{k}_i-\mathbf{k}_L)\delta(\mathbf{k}_j-\mathbf{k}_L) + \langle B_S(\mathbf{k}_i)B_S(\mathbf{k}_j)^*\rangle. \tag{36}$$

Equating this result with the right hand side of (35) yields the following expression for the initial (inhomogeneous) two-wave-vector correlation of the local random sea state:

$$\begin{aligned}\langle B_S(\mathbf{k}_i)B_S(\mathbf{k}_j)^*\rangle &= C(\mathbf{k}_i)\delta(\mathbf{k}_i-\mathbf{k}_j)\\ &- B_L\frac{V^{(1)}_{\mathbf{k}_i,\mathbf{k}_L,\mathbf{k}_j}+V^{(1)}_{\mathbf{k}_i,\mathbf{k}_j,\mathbf{k}_L}}{\omega(\mathbf{k}_i)-\omega(\mathbf{k}_L)-\omega(\mathbf{k}_j)}C(\mathbf{k}_j)\,\delta(\mathbf{k}_i-\mathbf{k}_j-\mathbf{k}_L)\\ &- B_L^*\frac{V^{(1)}_{\mathbf{k}_j,\mathbf{k}_L,\mathbf{k}_i}+V^{(1)}_{\mathbf{k}_j,\mathbf{k}_i,\mathbf{k}_L}}{\omega(\mathbf{k}_j)-\omega(\mathbf{k}_L)-\omega(\mathbf{k}_i)}C(\mathbf{k}_i)\,\delta(\mathbf{k}_j-\mathbf{k}_i-\mathbf{k}_L)\\ &- B_L^*\frac{V^{(2)}_{\mathbf{k}_i,\mathbf{k}_L,\mathbf{k}_j}}{\omega(\mathbf{k}_i)+\omega(\mathbf{k}_L)-\omega(\mathbf{k}_j)}C(\mathbf{k}_j)\,\delta(\mathbf{k}_i-\mathbf{k}_j+\mathbf{k}_L)\\ &- B_L\frac{V^{(2)}_{\mathbf{k}_j,\mathbf{k}_L,\mathbf{k}_i}}{\omega(\mathbf{k}_j)+\omega(\mathbf{k}_L)-\omega(\mathbf{k}_i)}C(\mathbf{k}_i)\,\delta(\mathbf{k}_j-\mathbf{k}_i+\mathbf{k}_L).\end{aligned} \tag{37}$$

Note that this equation correlates, at $t = 0$, waves that satisfy the relation $\mathbf{k}_i - \mathbf{k}_j = \pm\mathbf{k}_L$. This equation is the end result of this section.

5.2 Numerical simulations

From now on, due to the complexity of the numerical computations involved, we restrict ourselves to waves propagating in one dimension for both the sea state and the swell. We begin by discretizing the C.S.Y. Eq. (7) as follows.

The discretization consists in defining a numerical wave number space of $N = 600$ evenly spaced Fourier modes on the interval $[4/N, 4]$, since the peak wave $k_p = 1$. Then one replaces the continuous two-wave vector correlation function by a discrete sum of deltas

$$R_{ij}(t) = \sum_{n,m=1}^{N} R_{nm}(t)\delta(k_n - k_i)\delta(\mathbf{k}_m - \mathbf{k}_j), \tag{38}$$

where $R_{nm}(t)$ is a discrete complex valued function; the correlation between the amplitudes B_n and B_m at time t. Note that correlations between complex amplitudes of waves outside the numerical grid are not taken into account by the delta functions.

The time evolution of the discrete correlation function (38) is governed by the following non-linear system of O.D.E. called the discretized C.S.Y. equation:

$$\begin{aligned}\frac{d}{dt}R_{ij} &= -2i\sum_{m,n,p=1}^{N} T_{i,m,n,p}\delta^{n,p}_{i,m}e^{i\Delta^{n,p}_{i,m}t}R_{nj}R_{pm}\\ &+ 2i\sum_{m,n,p}^{N} T_{j,m,n,p}\delta^{n,p}_{j,m}e^{-i\Delta^{n,p}_{j,m}t}R_{in}R_{mp}.\end{aligned} \tag{39}$$

Here $\delta^{n,p}_{j,m}$ stands for the Kronecker's delta.

This system is complemented with the following initial data. One uses Eq. (27) for the initial wave action spectrum:

$$R_{ij}(0) = C_i, \quad \text{for} \quad i = j = 1, \ldots, N. \tag{40}$$

Author's personal copy

Initial inhomogeneous terms are obtained by discretizing equation (37), i.e. by selecting only the correlations between the waves in the numerical domain. This is achieved by substituting (19) into (37) and upon manipulations with the delta functions involved one reaches the following equation:

$$R_{ij}(0) = S_{ij}^{(1)} + S_{ij}^{(2)} + S_{ij}^{(3)} + S_{ij}^{(4)}, \quad \text{for} \quad i \neq j. \tag{41}$$

Where each of the terms is given below:

$$S_{ij}^{(1)} = \begin{cases} -B_L \dfrac{V^{(1)}_{k_j+k_L,k_L,k_j} + V^{(1)}_{k_j+k_L,k_j,k_L}}{\omega(k_j+k_L)-\omega(k_L)-\omega(k_j)} C_j(0) \\ \text{for } k_j = k_1, \ldots, k_N \text{ and } k_i = k_j + k_L. \\ 0, \text{ otherwise.} \end{cases}$$

$$S_{ij}^{(2)} = \begin{cases} -B_L^* \dfrac{V^{(1)}_{k_i+k_L,k_L,k_i} + V^{(1)}_{k_i+k_L,k_i,k_L}}{\omega(k_i+k_L)-\omega(k_L)-\omega(k_i)} C_i(0) \\ \text{for } k_j = k_1, \ldots, k_N \text{ and } k_i = k_j - k_L. \\ 0, \text{ otherwise.} \end{cases}$$

$$S_{ij}^{(3)} = \begin{cases} -B_L^* \dfrac{V^{(2)}_{k_i-k_L,k_L,k_i}}{\omega(k_i-k_L)+\omega(k_L)-\omega(k_i)} C_i(0) \\ \text{for } k_j = k_1, \ldots, k_N \text{ and } k_i = k_j - k_L. \\ 0, \text{ otherwise.} \end{cases}$$

$$S_{ij}^{(4)} = \begin{cases} -B_L \dfrac{V^{(2)}_{k_i-k_L,k_L,k_i}}{\omega(k_i-k_L)+\omega(k_L)-\omega(k_i)} C_i(0) \\ \text{for } k_i = k_1, \ldots, k_N \text{ and } k_j = k_i - k_L. \\ 0, \text{ otherwise.} \end{cases}$$

From now on, the wave number of the swell k_L under consideration also lies in the numerical grid.

Finally, the initial complex amplitude of the swell is related to the physical amplitude of the wave a_L by

$$|B_L|^2 = \frac{2g\pi^2}{\omega_L} a_L^2, \tag{42}$$

One also needs to specify an initial phase θ_L. In all our numerical simulations shown here, the value of the phase is $\theta_L = 0$, in which case $B_L = |B_L|$.

The evolution of the wave action spectrum R_{jj} and the variance $\rho(x,t)$ do not depend on the initial phase θ_L. It only affects the evolution of two-wave vector correlations of the form R_{ij} for $i \neq j$.

The parameters of the different JONSWAP spectra, together with the parameters of the swell are given in Table 1.

The choice of parameters α and γ in cases A was taken from case B4 in Ribal et al. (2013). Cases B correspond to the most unstable case found in Andrade and Stiassnie (2020).

As was mentioned above, by choosing N wave numbers in the numerical grid, one ends up with a number of two-wave vector correlations of $\mathcal{O}(N^2)$, to be evolved in time. Nevertheless, as was pointed out in Andrade and Stiassnie (2020), during the time evolution not all the possible correlations are activated. The only correlations that participate in the long-time evolution have the form R_{ij} where

$$k_i - k_j = nk_L, \quad \text{for some integer } n. \tag{43}$$

Here k_L is the wave number of the swell, which also has to be on the numerical grid.

This observation allows us to work efficiently with a smaller number of two-wave number correlations. For instance for case $A3$ the wave vector of the swell is $k_L = 0.34 = 51dk$, with $dk = 4/600$. The number of two-wave correlations was dramatically reduced[3] from 180,300 to 3834.

The time integration of Eq. (39) is computed with MATLAB's ode45 routine with relative and absolute tolerances set to 10^{-12}. The accuracy of the numerical solver can be seen from the conservation of the invariants associated with the discrete C.S.Y. equation namely, wave action A, momentum $\mathbf{M}$ and $\tilde{H}$, see Andrade and Stiassnie (2020) or Appendix B. Note that the invariants depend only on the initial spectrum, not on k_L. In cases A1–A5 the values of the invariants are $A = 1.90$, $\mathbf{M} = 2.10$ and $\tilde{H} = 6.19$ and in cases B1–B5 are $A = 1.54$, $\mathbf{M} = 1.64$ and $\tilde{H} = 4.94$.

In the following sections we present numerical simulations of non-linear, long-time evolution. Our main results are the evolution of the wave action spectrum, the evolution of the variance of the free surface and an increase in the probability of freak wave occurrence.

6 Results for the wave action spectrum

Once the time evolution of the correlation function is computed, we analyze the evolution of the wave action spectrum $R_{jj}(t)$.

In Figs. 3 and 4 we plot the long time evolution of the wave action spectrum for each case. Note that we use the dimensionless time variable $\tilde{t} = (\varepsilon^2\omega_p)t$. In all cases the final time is $\tilde{t} = 150$, which corresponds to about 700 peak periods for cases A and about 900 peak periods for cases B. In the plots the spectrum was normalized with respect to the initial wave action at the peak wave k_p:

[3] Taking the symmetry $R_{ij} = R_{ji}^*$ into account.

Author's personal copy

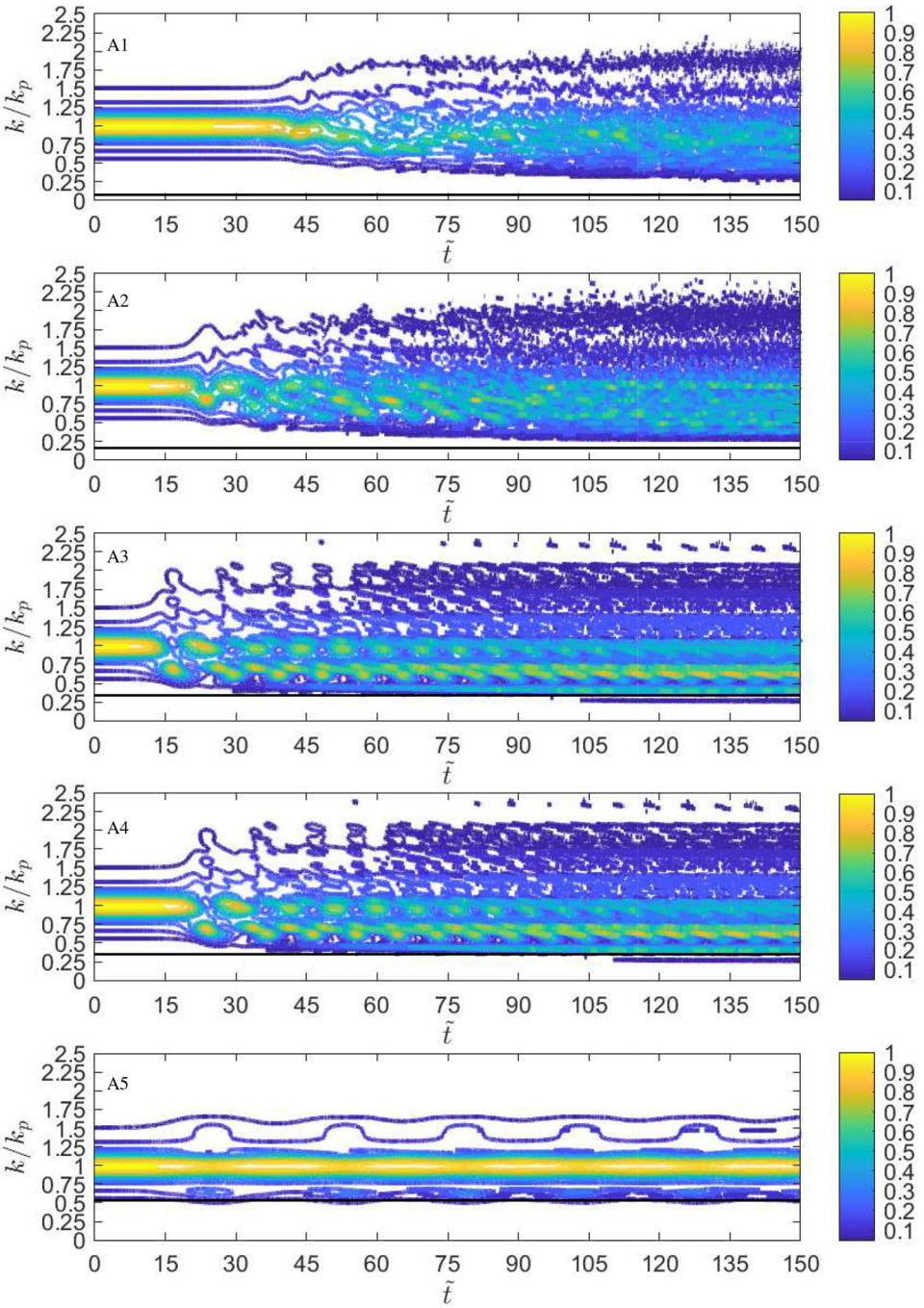

Fig. 3 Long time evolution of the wave action spectrum R_{jj}/C_p. Cases A1–A5 from top to bottom. The black solid line shows the wave number of the swell k_L

$$C_p = \frac{4g\pi^2\alpha\gamma e^{-5/4}dk}{2k_p^3\omega_p}. \tag{44}$$

Initially, the evolution of the spectrum is qualitatively similar in all cases considered here. There is a "warm-up" period where there is no visible spectral evolution whatsoever. It is followed by an energy exchange between the peak wave and neighboring waves. Although the energy going to both sides of the peak wave, there is a significant down shift, i.e. a significant portion of the energy goes to waves with smaller wave numbers. Then the effect of the wave number of the perturbation k_L becomes visible.

When k_L is small, the warm up is followed by a fast broadening of the spectrum, with the bulk of the energy being mixed among neighboring longer waves. This can be seen from the first two panels in Figs. 3 and 4 corresponding to cases A1, A2, B1 and B2, respectively.

Cases A3, and B3 were chosen so that k_L causes the fastest growth rate in each case. In these cases the energy exchange follows a different pattern. The bulk of the energy

Author's personal copy

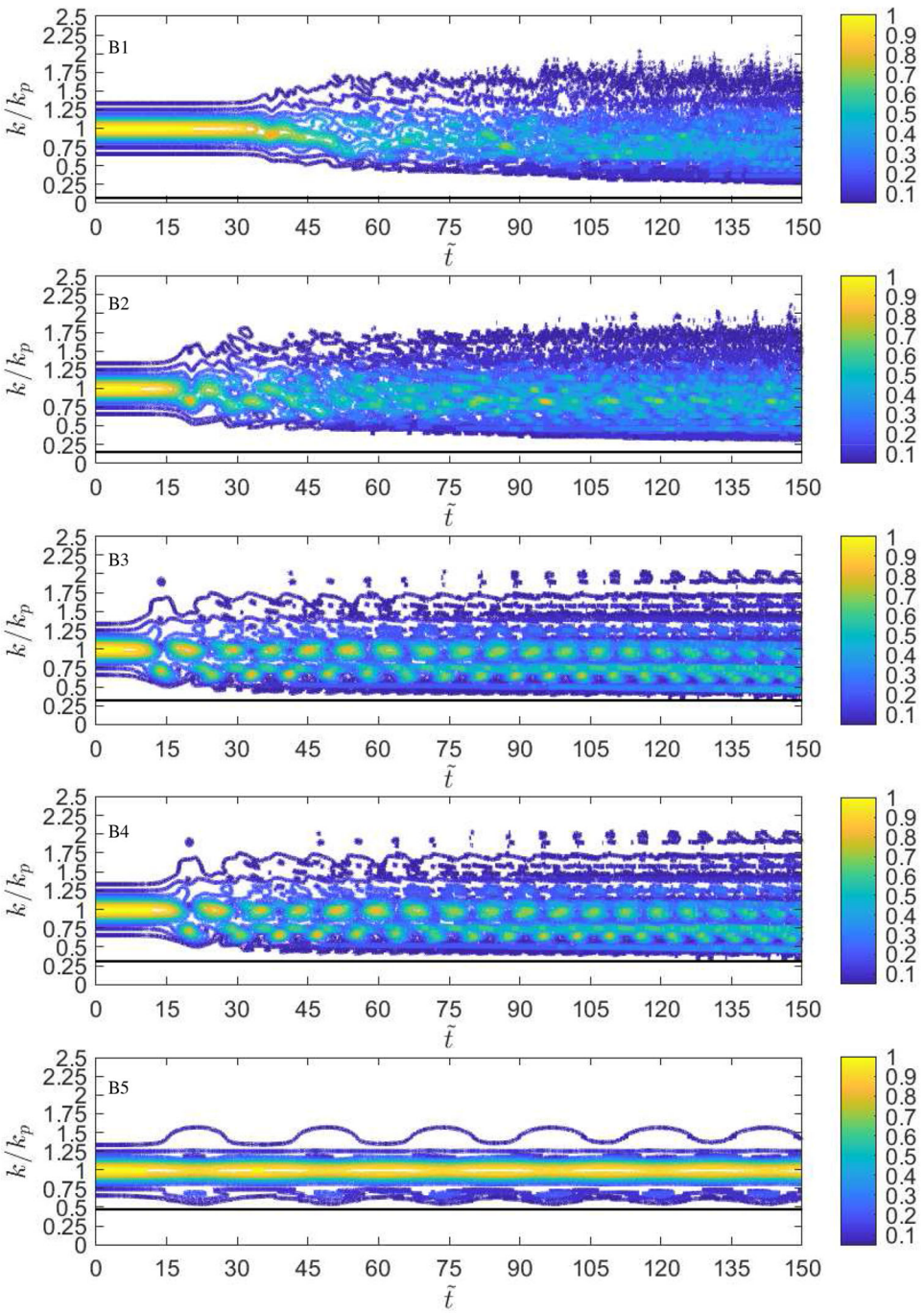

Fig. 4 Long time evolution of the wave action spectrum R_{jj}/C_p. Cases B1–B5 from top to bottom. The black solid line shows the wave number of the swell k_L

is exchanged back and forth between the peak and neighboring (longer) waves with some energy leaking out to shorter waves accounting for an overall broadening of the spectrum.

A similar behavior is observed in cases A4 and B4. These cases used the same wave vector of the swell as A3 and B3 did. The only difference being the amplitude of the initial swell. From 1 cm it was dropped down to 1 mm. Aside from a longer warm-up period, the evolution of these cases is practically indistinguishable from those of cases A3 and B3.

Finally cases A5 and B5, characterized by having the largest k_L, also exhibit a different type of behavior from all the previous cases. This time the bulk of the energy remains around the peak wave with little energy being exchanged, in a recurrent manner, among neighboring waves.

We point out that as the wave number of the swell increases, k_L leaves the instability region, see Figs. 1 and 2, thus stabilizing the system. From the spectral time evolution point of view, the wave action spectrum would become stationary. Despite this fact, it is interesting to see that for

Author's personal copy

cases A5 and B5, cases where k_L sits inside the instability region, there is some kind of stabilization effect taking place. There is little spectral evolution as compared to any of the other cases.

One possible explanation of this effect is the following. When k_L is small, the bound-waves introduce correlations between waves that are close to one another. This type of correlations among the waves seems to facilitate the energy exchange among the wave components leading to a broadening of the spectrum as seen especially in cases A1, A2, B1 and B2. On the other hand, when k_L is large and as the spectrum is narrow, the bound-waves are correlating waves inside the spectrum with waves that have little energy outside of it. Note that the evolution is almost periodic in cases A5 and B5 somewhat resembling the recurrent behavior in the Benjamin–Fier instability, see Mei et al. (2018).

7 Results for the variance of the free surface

Now we turn to the variance of the free surface elevation which can be computed from R_{ij} as:

$$\rho(x,t) = \frac{1}{8g\pi^2}\sum_{i,j=1}^{N}\sqrt{\omega_i\omega_j}\left[R_{ij}e^{i((k_i-k_j)x-(\omega_i-\omega_j)t)} + c.c.\right] \tag{45}$$

This equation is obtained by averaging the square of the free surface elevation, so it is proportional to the average wave energy of the wave field, see Holthuijsen (2010). Details on the derivation of Eq. (45) can be found in Andrade and Stiassnie (2020).

There are two properties of the variance. First, it is a periodic function of x with period $2\pi/k_L$. Second, in the homogeneous case the variance is constant. We denote it in this case as

$$\rho_h = \frac{1}{4g\pi^2}\sum_{j=1}^{N}\omega_j C_j. \tag{46}$$

The value of the homogeneous variance is used to normalize the variance thus showing how the energy changes with respect to that of the homogeneous unperturbed sea state.

We introduce the following dimensionless variables:

$$\tilde{x} = (\varepsilon k_p)x. \tag{47}$$

$$\tilde{\rho} = \rho/\rho_h. \tag{48}$$

Owing to the spatial periodicity of the variance and in order to highlight its time evolution, we have shifted $\tilde{\rho}$ periodically (in $\tilde{x}$) so that its maximum appears always towards the edge of the figure. The level lines of the variance are plotted in Fig. 5 for cases A1–A5 and in Fig. 6 for cases B1–B5.

In cases A1, A2, B1 and B2 the variance shows a manifestation of the apparent "turbulent" structure of the spectrum. This type of behavior has not been observed before in neither studies of solutions of the C.S.Y. equation nor in solutions of the Alber's equation.

The time evolution of the variance of cases A3, A4, B3 and B4 follows the following pattern. Their level lines form a sequence of circular shapes, with centers towards the upper and lower edges of the figures, showing a local concentration of wave energy. As the time evolution progresses, these level lines flat out, indicating that the wave field reaches a state of continuous concentration of energy. These results were recently reported in Andrade and Stiassnie (2020).

In all the cases treated so far, the evolution of the variance behaves differently to what was predicted by Alber's equation, despite the fact that the initial wave action spectrum is narrow. Previous results concerning the evolution of the variance, see Stiassnie et al. (2008), Regev et al. (2008) or Ribal et al. (2013), show that its evolution is recurrent in *time*. This is certainly the main difference between solutions of the C.S.Y. equation and Alber's equation.

The variance of cases A3, A4, B3 and B4 also reveals that the amplitude of the swell merely changes the warm-up period before the energy exchange. A similar behavior has been observed by Stuhlmeier and Stiassnie in the evolution of degenerated quartets of waves, see Stuhlmeier and Stiassnie (2019).

Cases A5 and B5 also show a different behavior. Their variance displays a recurrent pattern typical of solutions of Alber's equation. Moreover one can see how the variance corresponds to the evolution of its spectrum.

8 Results for the freak-wave statistics

The results of the previous sections are used to compute the probability of the wave height H exceeding a value H_0, on an interval $[0, L]$ during a time window $[0, T]$. These probabilities depend on the time evolution of the dimensionless variance $\tilde{\rho}$. They are computed by:

$$P(H > H_0) = \frac{1}{LT}\int_0^L\int_0^T \exp\left(-\left(\frac{H_0}{H_{rms0}}\right)^2\frac{1}{\tilde{\rho}(x,t)}\right)dxdt. \tag{49}$$

Here H_{rms0} denotes the RMS (root mean square) wave height of the homogeneous case. It is related to the (constant) homogeneous variance ρ_h by:

$$H_{rms0} = \sqrt{8\rho_h}. \tag{50}$$

Author's personal copy

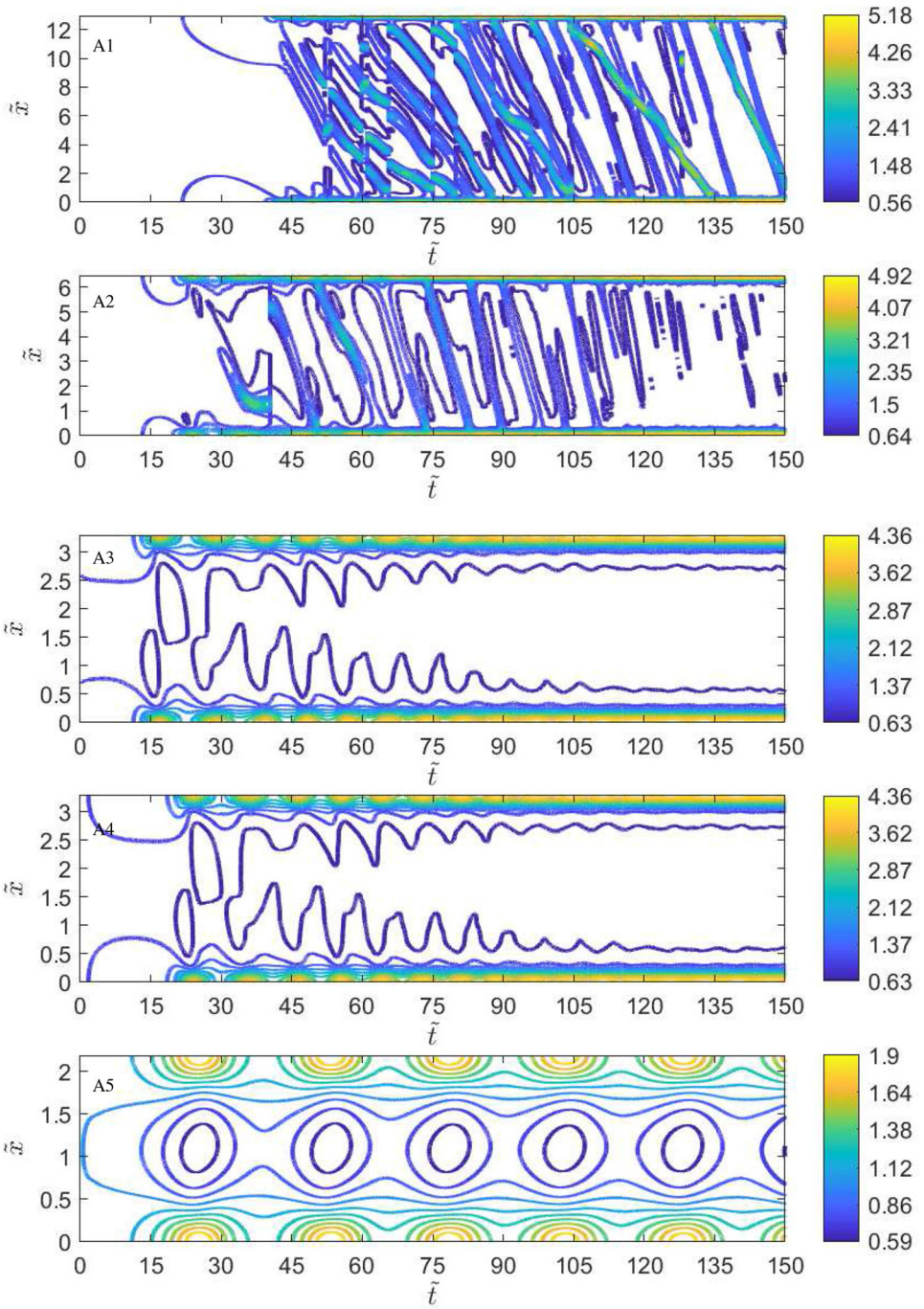

Fig. 5 Long time evolution of the variance of the free surface $\rho(x,t)/\rho_h$. Cases A1–A5 from top to bottom

Note that in the homogeneous case $\tilde{\rho} = 1$ and equation (49) reduces to the Rayleigh distribution

$$P(H > H_0) = \exp\left(\left(-\frac{H_0}{H_{rms0}}\right)^2\right). \tag{51}$$

In what follows, owing to the spatial periodicity of the variance, L is set to one period and the time window under consideration is $[0, \tilde{T} = 150]$. In this case Eq. (49) can be shown to be equivalent to that originally derived by Regev et al. (2008) and used in Ribal et al. (2013).

As our current interest is the probability of encountering freak waves, we need an estimate for the significant wave height H_s. Following Holthuijsen (2010), H_s is readily estimated from the spectrum as $H_s = 4\sqrt{m_0}$, where $\sqrt{m_0}$ is the standard deviation of the surface elevation, i.e. $\sqrt{m_0} = \sqrt{\rho_h}$. Thus the following relation holds

$$H_s = \sqrt{2} H_{rms0}. \tag{52}$$

Author's personal copy

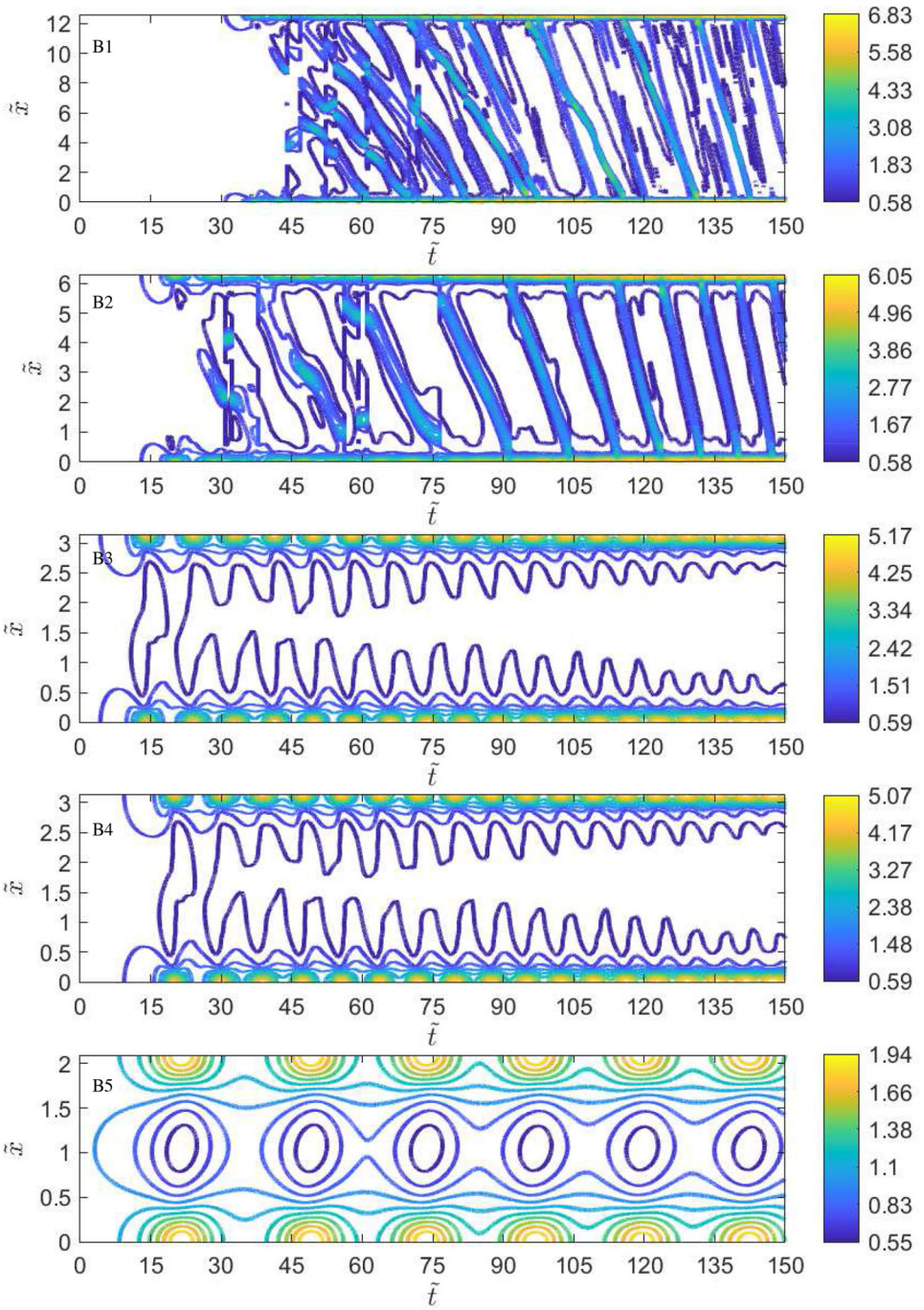

Fig. 6 Long time evolution of the variance of the free surface $\rho(x,t)/\rho_h$. Cases B1–B5 from top to bottom

In Fig. 7 we plot the probability of encountering freak waves, namely: the probability of wave heights exceeding two times the significant wave height H_s. Precise values are given in Table 2. The upper panel corresponds to cases A and the lower panel to cases B.

By looking at the freak-wave probabilities of cases A1–A4 and B1–B4, one can see that they are significantly higher than those of cases A5 and B5. In any case they are much higher than the probabilities taken from the Rayleigh distribution. Note that the variances of cases A1–A4 and B1–B4, reach values of about four to six times the energy of the unperturbed homogeneous wave field. The regions where such concentration of energy happens are the breeding ground for extreme waves. The fact that throughout the evolution there are many of such high energy regions, manifest itself in the statistics as an increase in the probability of freak wave occurrence.

Note that the probabilities for cases A3, A4, as well as B3 and B4 almost overlap with each other. This small discrepancy is due to the relatively longer warm up period in A4 and B4 as opposed to that of A3 and B3 respectively.

Author's personal copy

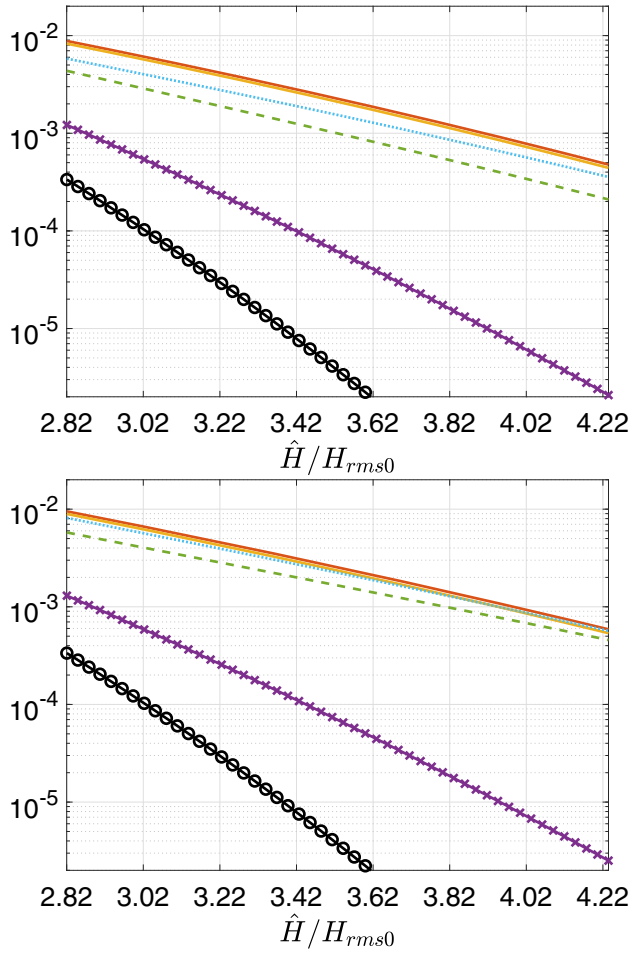

Fig. 7 Freak wave probabilities. Top panel: cases A1–A5. Bottom panel: cases B1–B5. A1 and B1: green broken line. A2 and B2: blue dotted line. A3 and B3: red solid line. A4 and B4: yellow solid line. A5 and B5: Purple line with crosses. Rayleigh distribution in black line with circles

On the other hand, the variances of cases A5 and B5 reach smaller values, barely twice the energy of the undisturbed wave field. The fact that the energy concentration is lower reflects in the somewhat smaller freak-wave probabilities for these cases.

Finally, we point out that without the swell, i.e. if $B_L = 0$, there is no spectral evolution, the variance is stationary $\rho(x,t) = \rho_h$ and Eq. (49) becomes the Rayleigh distribution, Eq. (51).

9 Summary

The goal of this article was to study a physical mechanism capable of triggering the formation of freak-waves. This mechanism is based on the non-linear, long time evolution of an inhomogeneous instability, and its trigger is the initial two-wave vector correlation coming from the bound-waves (between the sea and the swell).

Table 2 Probabilities of encountering freak waves in each case

Cases	$P(H > 2H_s)$	$P(H > 3H_s)$
Case A1	0.0043	0.0002
Case A2	0.0058	0.0003
Case A3	0.0082	0.0004
Case A4	0.0088	0.0005
Case A5	0.0012	2.4×10^{-6}
Case B1	0.0057	0.0004
Case B2	0.0081	0.0006
Case B3	0.0089	0.0005
Case B4	0.0094	0.0006
Case B5	0.0013	2.9×10^{-6}
Rayleigh	0.0003	1.2×10^{-8}

Our new approach of finding the instability region of the spectrum, by means of the integral Eq. (18), is an improvement over the method used in Andrade and Stiassnie (2020); as it allows to treat oblique and even opposing swells in the inhomogeneous disturbance.

We point out that, by choosing a wave vector $\mathbf{k}_L$, the initial disturbance (17) is no more than a correlation between the random complex amplitudes $B(\mathbf{k})$ with $B(\mathbf{k} \pm \mathbf{k}_L)$. As our results are based on a broad-banded model there is no a priori restriction on $\mathbf{k}_L$. On the other hand, when using a narrow banded model, the waves $\mathbf{k}$ and $\mathbf{k} \pm \mathbf{k}_L$ have to be close to each other, a condition that in principle forces $\mathbf{k}_L$ to be small.

The examples treated here were all unstable to small wave vectors $\mathbf{k}_L$, suggesting that not only a swell may trigger the generation of freak-waves, but also infra gravity waves:long frequency waves generated for example by triad interactions of shoaling waves and their coastal reflections, see Rawat et al. (2014).

It should be noted that the initial inhomogeneous disturbance, used to initialize the time evolution, i.e. Eq. (37), comes from the bound-waves, not from solving Eq. (18) for some λ and some function M. Nevertheless, from the time evolution, we see that the bound-waves successfully trigger the instability.

In this article we dealt with narrow, hence unstable, JONSWAP spectrum as indicated by the values of the peakedness parameter of the spectrum $\gamma = 10$ and 20. In the ocean, smaller values of γ, between 1 and 3 are more common. For the values of the parameter α used in our examples, a JONSWAP spectrum, with these smaller values of γ, is stable. This result was also obtained by Ribal et al. (2013) and Gramstad (2017) using Alber's equation. A plot of the instability region of the JONSWAP spectrum in the $(\gamma, \alpha)-$plane can be found in Fig. 2a of Andrade and Stiassnie (2020).

Author's personal copy

For the cases where the spectrum is stable we saw no noticeable change in the non linear spectral evolution. Likewise, there was little change in the evolution of the variance of the free surface and the statistics, of the underlying sea state, closely followed the Rayleigh distribution. In other words, the mechanism of freak wave generation that we studied does not work in broad-banded sea states.

The C.S.Y. equation and its linearization, Eq. (10), can be used to study any type of wave spectrum. Despite of this generality, and due to the increasing complexity of the numerical calculations involved, we did not study a fully two dimensional case. The cases chosen for non-linear time evolution were one dimensional and were chosen so that we could compare with the results in Andrade and Stiassnie (2020).

One way of looking at our results is the following. Let us assume that there is a local sea state propagating towards the coast line, generated for instance by an offshore storm. Such sea state is destabilized by the bound-waves generated by either a following swell or, by reflections from the shoreline. Provided that the duration of the storm is long enough, so that sea state is maintained, there is a period of no big changes in the ocean (the warm-up period) and then, depending on the particular characteristics of the sea and the swell, it would develop regions of high wave energy, where one should expect to encounter extreme waves.

Acknowledgements This research was supported by the Israel Science Foundation, Grant 261/17.

Compliance with ethical standards

Conflict of interest The authors declare that they have no conflict of interest.

Appendix A

In this appendix we show the derivation of the discrete system of Eqs. (21) and (22), from the continuous equation (18), assuming a wave action spectrum of the form (19) and any wave vector $\mathbf{k}_L$.

To start with, note that by substituting Eq. (19) into (11) and integrating, the frequency Ω becomes:

$$\Omega_0 = \omega_0 + 2\sum_{j=1}^{N} T_{0,j,0,j} C_j. \tag{53}$$

Then we use an ansatz for M, see Eq. (20). This is motivated by the following. If one substitutes Eq. (19) into the right hand side of Eq. (18) the result would be a sum of Dirac deltas, supported on the points $\mathbf{m} \pm \mathbf{k}_L/2$. On the other hand substituting (19) into the left hand side of (18) gives a continuous function. The equality can only be fulfilled if $M(\mathbf{m})$ itself is a sum of Dirac deltas, supported on the points $\mathbf{m} \pm \mathbf{k}_L/2$. Any such sum of deltas can be written as (20).

Substituting (19) and (20) into the left hand side of (18) yields:

$$\begin{aligned}\text{L.H.S.} = &\sum_{j=1}^{N} \left(\lambda + \Omega_j + \Omega_{j-k}\right) M_j^m \delta(\mathbf{m} - \mathbf{k}_j + \mathbf{k}_L/2) \\ &+ \sum_{j=1}^{N} \left(\lambda + \Omega_{j+k} - \Omega_j\right) M_j^p \delta(\mathbf{m} - \mathbf{k}_j - \mathbf{k}_L/2).\end{aligned} \tag{54}$$

On the other hand, the right hand side of (18) becomes

$$\begin{aligned}\text{R.H.S.} = &2\sum_{j=1}^{N} C_j I(\mathbf{k}_j - \mathbf{k}_L/2)\delta(\mathbf{m} - \mathbf{k}_j + \mathbf{k}_L/2) \\ &- 2\sum_{j=1}^{N} C_j I(\mathbf{k}_j + \mathbf{k}_L/2)\delta(\mathbf{m} - \mathbf{k}_j - \mathbf{k}_L/2).\end{aligned} \tag{55}$$

Where I denotes the integral of the kernel

$$\begin{aligned}I(\mathbf{m}) &= \int T(\mathbf{m} + \mathbf{k}_L/2, \mathbf{u} - \mathbf{k}_L/2, \mathbf{m} \\ &\quad - \mathbf{k}_L/2, \mathbf{u} + \mathbf{k}_L/2) M(\mathbf{u})\, d\mathbf{u} \\ &= \sum_{j=1}^{N} M_j^m T(\mathbf{m} + \mathbf{k}_L/2, \mathbf{k}_j - \mathbf{k}_L, \mathbf{m} - \mathbf{k}_L/2, \mathbf{k}_j) \\ &\quad + \sum_{j=1}^{N} M_j^p T(\mathbf{m} + \mathbf{k}_L/2, \mathbf{k}_j, \mathbf{m} - \mathbf{k}_L/2, \mathbf{k}_j + \mathbf{k}_L).\end{aligned} \tag{56}$$

Finally one equates all the terms in (54) with those of (55), according to their corresponding delta function. This results in the following $2N$ system of equations, for M_i^m and M_i^p and $i = 1, \ldots, N$:

$$\begin{aligned}&(\lambda + \Omega_i - \Omega_{i-k})\, M_i^m \\ &\quad = 2C_i \sum_{j=1}^{N} M_j^m T_{i,j-k,i-k,j} + M_j^p T_{i,j,i-k,j+k}.\end{aligned} \tag{57}$$

$$\begin{aligned}&(\lambda + \Omega_i + k - \Omega_i)\, M_i^p \\ &\quad = -2C_i \sum_{j=1}^{N} M_j^m T_{i+k,j-k,i,j} + M_j^p T_{i+k,j,i,j+k}.\end{aligned} \tag{58}$$

Recall that the subscript k stands for the wave vector $\mathbf{k}_L$ thus, $T_{i,j-k,i-k,j} = T(\mathbf{k}_i, \mathbf{k}_j - \mathbf{k}_L, \mathbf{k}_i - \mathbf{k}_L, \mathbf{k}_j)$, etc. These are Eqs. (21) and (22) respectively.

Author's personal copy

Appendix B

In this appendix we give the invariants of the C.S.Y. equation namely, wave action A, momentum $\mathbf{M}$ and a third invariant $\tilde{H}$, related to the Hamiltonian.

The invariants are

$$A = \int R_{jj}\, d\mathbf{k}_j. \tag{59}$$

$$\mathbf{M} = \int \mathbf{k}_j R_{jj}\, d\mathbf{k}_j. \tag{60}$$

$$\tilde{H} = \int \omega_j R_{jj}\, d\mathbf{k}_j - \iiiint T_{j,m,n,p}\delta^{n,p}_{j,m}\Delta^{n,p}_{j,m} \times \int_0^t \mathrm{Im}\left(e^{i\Delta^{n,p}_{j,m}s} R_{nj} R_{pm}\right) ds\, d\mathbf{k}_{j,m,n,p}. \tag{61}$$

The invariants of the discrete C.S.Y. equation are formally obtained by replacing the integrals by discrete sums.

References

Alber IE (1978) The effects of randomness on the stability of two-dimensional surface wavetrains. Proc R Soc A Math Phys Eng Sci 363(1715):525–546. https://doi.org/10.1098/rspa.1978.0181 ISSN 1364-5021

Andrade D, Stiassnie M (2020) New solutions of the C.S.Y. equation reveal increases in freak wave occurrence. Wave Motion. https://doi.org/10.1016/j.wavemoti.2020.102581

Athanassoulis AG, Athanassoulis GA, Sapsis TP (2017) Localized instabilities of the Wigner equation as a model for the emergence of rogue waves. J Ocean Eng Mar Energy 3(4):353–372

Badulin SI, Shrira VI, Kharif C, Ioualalen M (1995) On two approaches to the problem of instability of short-crested water waves. J Fluid Mech 303:297–326

Crawford DR, Saffman PG, Yuen HC (1980) Evolution of a random inhomogeneous field of nonlinear deep-water gravity waves. Wave Motion 2(1):1–16. https://doi.org/10.1016/0165-2125(80)90029-3 **(ISSN 0165-2125)**

Gramstad O (2017) Modulational instability in Jonswap sea states using the Alber equation. In: ASME 2017 36th international conference on ocean, offshoreand arctic engineering. American Society of Mechanical Engineers Digital Collection, Trondheim, Norway

Holthuijsen LH (2010) Waves in oceanic and coastal water. Cambridge University Press, Cambridge

Krasitskii VP (1994) On reduced equations in the Hamiltonian theory of weakly nonlinear surface waves. J Fluid Mech 272:1–20

Mei CC, Stiassnie MA, Yue DK-P (2018) Theory and applications of ocean surface waves: part 2: nonlinear aspects, 3rd edn. World Scientific, Singapore

Rawat A, Ardhuin F, Ballu V, Crawford W, Corela C, Aucan J (2014) Infragravity waves across the oceans. Geophys Res Lett 41(22):7957–7963

Regev A, Agnon Y, Stiassnie M, Gramstad O (2008) Sea swell interaction as a mechanism for the generation of freak waves. Phys Fluids 20(11):112102. https://doi.org/10.1063/1.3012542

Ribal A, Babanin AV, Young I, Toffoli A, Stiassnie M (2013) Recurrent solutions of the Alber equation initialized by joint north sea wave project spectra. J Fluid Mech 719:314–344. https://doi.org/10.1017/jfm.2013.7 **(ISSN 0022-1120)**

Stiassnie M, Regev A, Agnon Y (2008) Recurrent solutions of Alber's equation for random water-wave fields. J Fluid Mech. https://doi.org/10.1017/s0022112007009998 **(ISSN 0022-1120)**

Stuhlmeier R, Stiassnie M (2019) Evolution of statistically inhomogeneous degenerate water wave quartets. Philos Trans R Soc A Math Phys Eng Sci 376(2111):20170101. https://doi.org/10.1098/rsta.2017.0101 **(ISSN 1364-503X)**

Yuen HC, Lake BM (1982) Nonlinear dynamics of deep-water gravity waves. Adv Appl Mech 22:67–229. https://doi.org/10.1016/s0065-2156(08)70066-8

Publisher's Note Springer Nature remains neutral with regard to jurisdictional claims in published maps and institutional affiliations.